Photofragment Imaging of Kr_2 and ArKr van der Waals Molecules following Two-Photon Excitation

Albert J. R. Heck,[†,‡] David W. Neyer,[†] Richard N. Zare,[‡] and David W. Chandler*[,†]

Combustion Research Facility, Sandia National Laboratories, Livermore, California 94551-0969, and Department of Chemistry, Stanford University, Stanford, California 94305

Received: July 18, 1995; In Final Form: September 29, 1995[⊗]

Photofragment imaging is used to study the fragmentation and ionization dynamics of Kr_2 and ArKr upon absorption of two or more photons ($\lambda = 211-220$ nm). For Kr_2 two-photon-excited electronic states are studied that are in energy near Kr (5p) states. All studied Kr_2 two-photon-excited electronic states show competition between ionization and predissociation. The photofragment images also reveal higher order absorption processes in which three-photon absorption of the dimer is followed by dissociation into ground state and excited state Kr fragments. Dissociation after three-photon absorption leads to Kr photofragments, whose recoil can be described by a $\cos^2\theta$ distribution with respect to the polarization vector of the laser. For ArKr two, two-photon-excited, electronic bands are observed near Kr (5p) and Ar (4s) transitions. The two-photon-excited ArKr molecules dissociate exclusively into excited state Ar (4s) atoms concomitant with ground state Kr atoms. Therefore, both electronic bands are assigned to Ar*Kr states, i.e. excited states that correlate to Ar (4s) and Kr $^1S_0$ atomic asymptotes. The Ar photofragment ion images and the multiphoton ionization spectra show competition between ionization and predissociation of these two-photon-excited ArKr states. As with the Kr_2 dimer, the ion images also reveal higher order absorption processes in which three-photon absorption of ArKr is followed by dissociation into neutral Kr ground and Ar excited state fragments. The angular distributions of the fragments formed after predissociation at the two-photon resonant levels and after three-photon absorption are both anisotropic. The recoil of the Ar photofragments after three-photon absorption can be described by a $\cos^2\theta$ distribution with respect to the polarization vector of the laser. Markedly different contributions of three-photon absorption and predissociation processes are observed in the ion images of the two electronic bands of ArKr, i.e. three-photon absorption processes are more important than predissociation processes for the electronic band starting at 93 699 cm^{-1}, whereas predissociation processes are more important than three-photon absorption for the electronic band starting at 94 180 cm^{-1}.

Introduction

Rare-gas dimers have been the subject of considerable experimental study over the past decade, because of their use in vacuum ultraviolet (VUV) lasers.[1-4] Since the initial work by Mulliken,[5] the rare-gas dimers have also been the subject of continued theoretical interest.[6-9] Excited states of rare-gas dimers are all Rydberg-like states and typically have energies near corresponding atomic states. The lower excited states of several rare-gas molecules have been characterized spectroscopically using VUV absorption,[10] emission,[11] and laser-induced fluorescence (LIF)[12-15] techniques. More recently, resonantly enhanced multiphoton ionization (REMPI)[16-23] and two-photon LIF[24] have been used extensively to study the low-lying excited states of both homonuclear dimers such as Ar_2, Kr_2, and Xe_2 and heteronuclear dimers such as ArXe, KrXe, and ArKr. Excited states of Kr_2 and ArKr have also been examined by Eden and co-workers[25-28] using inter-Rydberg transient absorption spectroscopy from metastable triplet states.

Potential energy surfaces of Kr_2[8] and ArKr[7] have been calculated using *ab initio* methods. In the ground state of a rare-gas van der Waals molecule the two atoms typically repel each other, but van der Waals attractions can lead to weak binding. The ground states of Kr_2 and ArKr are similar. The Kr_2 ground state is bound by 0.0157 eV ($r_e = 4.017$ Å),[8,10,12] and the ArKr ground state is bound by 0.016 eV ($r_e = 3.9$ Å).[10]

Since the ionic core of the Rydberg states typically determines their behavior, it is worthwhile to examine the bonding properties within Kr_2^+ and $ArKr^+$ ions. Ionization of the Kr_2 and ArKr van der Waals molecules removes an electron from an antibonding orbital and thus leads to bound ionic ground states. The dissociation energy of the ground state of Kr_2^+ is 1.15 eV,[29,30] whereas that of $ArKr^+$ is only 0.5 eV[31,32] (for comparison, D_0 is 1.25 eV for Ar_2^+[29,33]). In general, ground state homonuclear rare-gas ions are much more strongly bound than ground state heteronuclear rare-gas ions. These different bonding characteristics stem from the much stronger interaction between the degenerate atomic orbitals in the homonuclear dimer than between the energetically separated orbitals in the heteronuclear dimer. Because the excited electronic states of these neutral dimers are Rydberg states, they may be described as ionic cores with an additional Rydberg electron. Therefore, the strong binding in some of the lower excited states of the homonuclear dimers is not surprising.

Excited electronic states of heavier rare-gas dimers are most often described using Hund's case c. More recently, however, Eden and co-workers[28] proposed that the electronic states are better described using Hund's case a. For easier comparison with the majority of previous studies we use Hund's case c to describe the electronic terms of the rare-gas dimers. In Hund's case c the molecular states are labeled by Ω, which is the projection of the total angular momentum J on the internuclear axis. For homonuclear dimers the states are labeled (u) and (g) depending on the inversion symmetry of the electronic wave function. This symmetry classification does not apply to

[†] Sandia National Laboratory.
[‡] Stanford University.
[⊗] Abstract published in *Advance ACS Abstracts*, November 15, 1995.

0022-3654/95/2099-17700$09.00/0

TABLE 1: Kr (5p) and Ar (4s) Atomic Transition Energies from the Ground State of Kr and Ar

	Racah notation	LS coupling notation	experimental energy (cm^{-1})	two-photon wavelength (nm)
Kr	$5p\,[1/2]_1$	$5p\,^3S_1$	91 169	219.37
	$5p\,[5/2]_3$	$5p\,^3D_3$	92 295	216.70
	$5p\,[5/2]_2$	$5p\,^3D_2$	92 308	216.67
	$5p\,[3/2]_1$	$5p\,^3D_1$	92 965	215.13
	$5p\,[3/2]_2$	$5p\,^1D_2$	93 124	214.77
	$5p'\,[1/2]_0$	$5p\,^3P_0$	94 093	212.56
	$5p'\,[3/2]_1$	$5p\,^1P_1$	97 596	204.92
Ar	$4s\,[3/2]^\circ_2$	$4s\,^3P_2$	93 144	214.72
	$4s\,[3/2]^\circ_1$	$4s\,^3P_1$	93 751	213.33
	$4s'\,[1/2]^\circ_0$	$4s\,^3P_0$	94 554	211.52
	$4s'\,[1/2]^\circ_1$	$4s\,^1P_1$	95 400	209.64

heteronuclear dimers. Additionally, the $\Omega = 0$ states are labeled 0^+ or 0^- depending on whether or not the electronic wave function changes sign upon reflection through the plane containing the nuclei. The electric dipole two-photon selection rules are $|\Delta\,\Omega| \leq 2$, $|\Delta\,J| \leq 2$, $g \leftrightarrow g$, $u \leftrightarrow u$, $0^+ \leftrightarrow 0^+$, and $0^- \leftrightarrow 0^-$, while $g \leftrightarrow u$ and $0^+ \leftrightarrow 0^-$ are forbidden. In Kr_2 the only allowed two-photon transitions from the 0_g^+ ground state are to the 0_g^+, 1_g, and 2_g states, and in ArKr from the 0^+ ground state to the 0^+, 1, and 2 states. For comparison the one-photon selection rules are $|\Delta\,\Omega| \leq 1$, $|\Delta\,J| \leq 1$, $g \leftrightarrow u$, $0^+ \leftrightarrow 0^+$, and $0^- \leftrightarrow 0^-$, while $g \leftrightarrow g$, $u \leftrightarrow u$, and $0^+ \leftrightarrow 0^-$ are forbidden. Therefore, the dipole allowed one-photon transitions are in ArKr from the 0^+ ground state to the 0^+ and 1 states.

Despite substantial spectroscopic data available on the electronic excited states of Kr_2 and ArKr, the assignment of observed transitions is far from complete. Several electronic bands, some of which display vibronic structure, have been observed near transitions to atomic Kr $4p^55p$ states and Ar $3p^54s$ states. Table 1 lists atomic Kr (5p) and Ar (4s) transition energies relevant to this study. Two-photon transitions in Kr_2 have been observed near the following atomic states: Kr $(5p)[3/2]_2$ (93 124 cm^{-1}),[19,23] Kr $(5p)[1/2]_0$ (94 093 cm^{-1}),[19,23] Kr $(5p)[5/2]_2$ (92 308 cm^{-1}),[20,23] and Kr $(5p)[5/2]_3$ (92 295 cm^{-1}).[20,23] Some of the transitions to these atomic states (for example, the transition to the Kr $(5p)[5/2]_3$ state) are two-photon forbidden. Combination of a ground state $^1S_0$ Kr atom with an excited state atom leads to $(J + 1)$ molecular states. Even excited atomic levels to which two-photon transitions are dipole forbidden can lead to several two-photon-allowed molecular states. Although the two-photon selection rules exclude some states, assignment of the observed transitions is complicated and has been, so far, only partly successful. In a two-photon REMPI study of the ArKr molecule Dehmer and Pratt[19] observed two electronic bands with different vibrational structure near the Kr $(5p)[3/2]_2$ atomic transition. Interestingly, these two bands are also very close to several Ar $3p^54s$ states. Tanaka et al.[10] observed less resolved transitions in a one-photon VUV absorption study. Both groups attribute these electronic transitions to excitations of the Kr atom within the molecule.

In this paper, we describe our investigations of the dissociation and ionization dynamics of two-photon-excited states of Kr_2 and ArKr near Kr (5p) and Ar (4s) atomic levels. More particularly, we reexamine, using the photofragment ion imaging technique,[34,35] the two-photon transitions observed by Echt et al.,[20] Dehmer and Pratt,[19] and Lipson et al.[23] for the Kr_2 dimer, and the two-photon transitions observed by Dehmer and Pratt[19] for the ArKr molecule. The ion-imaging technique[34,35] allows measurement of the three-dimensional velocity distribution of the photofragments. Determination of the speed and angular distributions of photofragments provides new insight into the dissociation and ionization dynamics of the studied two-photon-excited states of Kr_2 and ArKr.

Experimental Section

The photofragment ion imaging spectrometer has been described elsewhere in detail.[35-37] In brief, krypton or a mixture of krypton and argon (backing pressure 20 psig (375 kPa)) is expanded supersonically into a source vacuum chamber through a solenoid valve (General Valve series 9). Approximately 1 cm from the nozzle orifice, the beam is skimmed (Beam Dynamics, orifice 0.8 mm) and collimated by a hole (diameter 1 mm) in the repeller plate. The background pressure in the detection chamber is typically 10^{-6} Pa and increases to 10^{-5} Pa when the pulsed molecular beam is on. In the expansion, dimers and possibly higher order clusters are formed. The relative abundance of the dimers and higher clusters is unknown. Linearly polarized, tunable UV laser pulses are used to excite the dimers resonantly to two-photon-allowed excited states. The direction of the polarization vector is chosen to be parallel to the face of the position-sensitive ion detector. The UV light is generated by frequency doubling (Inrad) an injection-seeded Nd:YAG-pumped dye laser (Spectra Physics GCR5, PDL 2) using KD*P crystals. The frequency-doubled dye output is sum-frequency mixed (Inrad) with the residual dye laser output using appropriate BBO crystals. DCM dye dissolved in methanol is used. The bandwidth of the dye laser pulses is approximately 0.2 cm^{-1}. UV output powers are kept constant at 500 ± 30 μJ per pulse. The UV light is focused (f = 15 cm) into the molecular beam. After ionization, ions are accelerated along a 20-cm-long flight tube and impinge on a two-dimensional, position-sensitive detector. The detector consists of a pair of chevron microchannel plates (Galileo, 7.62 cm diameter) coupled to a fast phosphor screen (P47 Phosphor, 50-ns decay time). The laser, molecular beam, and detection system are all pulsed at 30 Hz. Timing is synchronized by digital delay generators (Stanford Research Systems). Research grade argon (99.9995%) and krypton (99.997%) were purchased from Spectra Gases (Newark, NJ). The argon−krypton mixture was prepared at an approximately 10:1 ratio.

To record REMPI spectra, mass selective detection of the ions is accomplished by setting boxcar gates on the appropriate mass peaks in the time-of-flight spectrum. The integrated phosphorescence on the detector is recorded using a photomultiplier tube. To record ion images, the laser is tuned to be resonant with a two-photon transition, and the front of the detector is pulsed to detect only one mass peak. The resulting images are recorded using a Peltier-cooled charge-coupled-device (CCD) camera (Photometrics, 576 × 384 pixels) equipped with a standard 50-mm lens (Pentax). Signal averaging is performed by opening the CCD camera shutter, for approximately 12 000 laser shots, to record a single image. The integrated charge on the CCD is read by the associated camera electronics and transferred for storage and processing to a MIPS RS3000 computer. Background subtraction is achieved using an image recorded with the laser firing well after the molecular beam gas pulse (typically 1-ms delay).

Results

Kr_2. Previously reported[19,20,23] two-photon resonances of Kr_2 in the 210−220-nm wavelength region were reproduced in our work. In Figure 1 part of the measured (2+1) REMPI spectrum of Kr_2 is shown. All observed transitions lead to Kr_2^+ and Kr^+ ions in the REMPI spectrum. Kr photofragment ion images were taken with the laser tuned to different vibrational bands of the observed electronic bands. In general, Kr photofragment

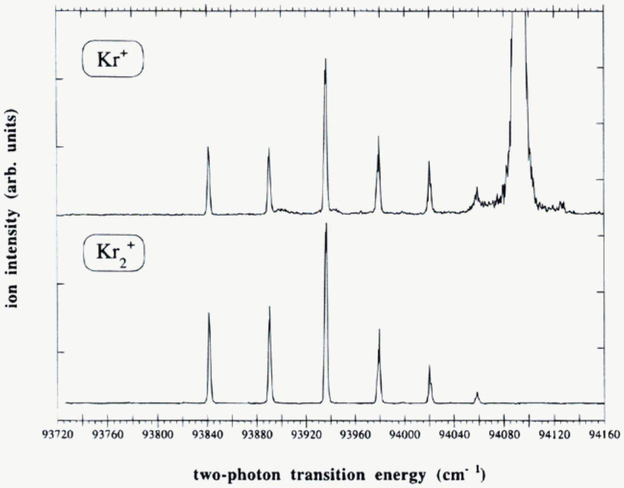

Figure 1. Two-photon resonant ionization spectra of Kr_2 and Kr, in the energy region near the Kr (5p) $[1/2]_0$ atomic transition.

ion images taken at different Kr_2 two-photon resonances are qualitatively similar. A typical Kr photofragment ion image is shown in Figure 2A. A significant contribution to the image comes from Kr atoms recoiling with low velocities, appearing at the center of the image. A second contribution comes from fast recoiling Kr photofragments. The speed distribution of the latter Kr photofragments is narrow, and their angular distribution can approximately be described by a $\cos^2 \theta$ distribution with respect to the laser polarization vector.

In Figure 1 the (2+1) REMPI spectrum of Kr_2 in the region of the Kr $^1S_0$ + Kr $(5p)[1/2]_0$ dissociation limit is shown. This spectrum displays the same features observed by Dehmer and Pratt[19] and Lipson et al.[23] for the Kr_2 ionization spectrum. An intense vibrational progression is observed. Lipson et al.[23] assigned the lowest observed vibrational level, at 93841 cm^{-1}, to $v' = 0$.[23] Table 2 lists the observed Kr_2^+ transitions of this electronic band. Kr^+ ions are formed in addition to Kr_2^+ ions at the two-photon resonances (see Figure 1). These Kr^+ signals are nearly as intense as the signals from the Kr_2^+ ions. The spectra in Figure 1 also display the strong two-photon-allowed Kr $^1S_0 \rightarrow$ Kr $(5p)[1/2]_0$ atomic transition.

In Figure 2A a photofragment ion image of Kr^+ ions is shown which was collected with the laser frequency tuned to a two-photon resonance of the dimer at 93 890 cm^{-1}, which corresponds to $v' = 1$ (see Table 2). An ion image is a two-dimensional projection of the three-dimensional velocity distribution of the photofragments. The three-dimensional speed distribution and angular distribution of the Kr photofragments are obtained from the inverse Abel transformed image.[35] In Figure 2B and Figure 2C, contour diagrams of the two-dimensional distributions are shown. The contour diagram in Figure 2C is identical to the one in Figure 2B, with the intensity multiplied by a factor of 15. The ion image shows an intense signal at the center that corresponds to Kr^+ ions with relatively low velocities. Additionally, the image shows a less intense outer ring with an anisotropic angular distribution that corresponds to Kr^+ ions with much higher velocities. Because the two channels do not overlap on the detector, the relative intensities can be obtained directly from the images. Although the outer ring seems weak, it covers a larger area than the inner ring, and the relative contributions to the image of the outer channel and the inner channel are 25% and 75%, respectively.

In Figure 3A an intensity plot along a single column of the CCD, parallel to the laser polarization vector and through the center of the image, is shown. By using the measured arrival time of the Kr^+ ions on the detector, we can convert the

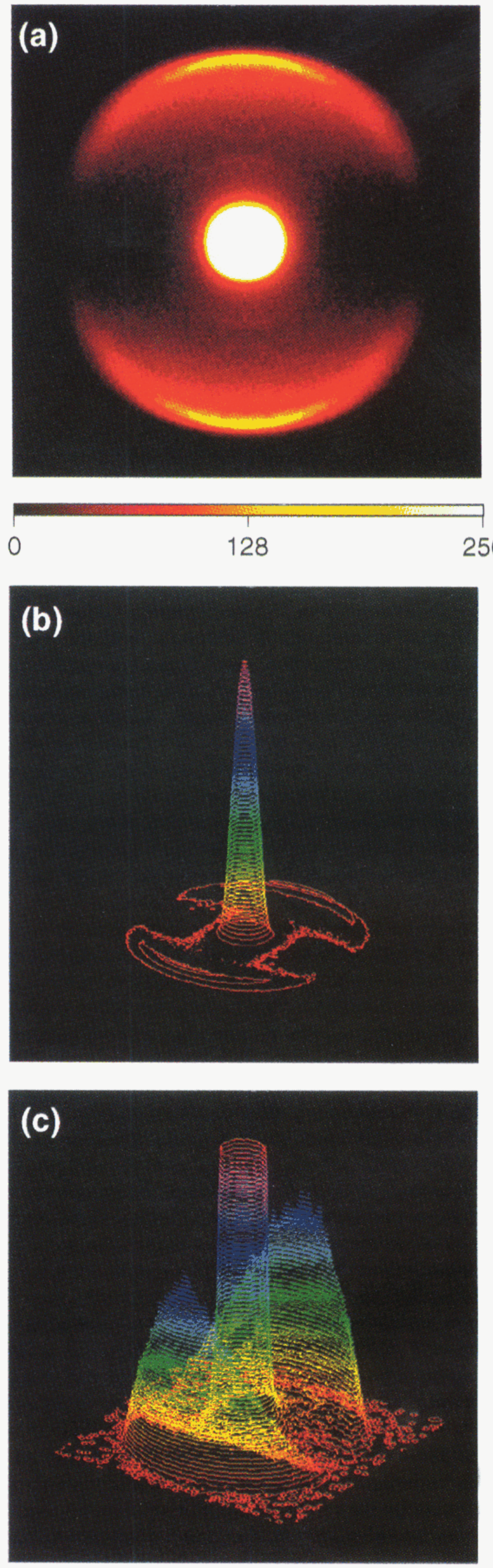

Figure 2. (a) Photofragment ion image of Kr, taken with the laser frequency at a two-photon resonance of the Kr_2 dimer at 93 890 cm^{-1}, which corresponds to the $v' = 1$ level in Table 2. (b) Velocity contour diagrams of Kr photofragments after resonant two-photon excitation at 93 890 cm^{-1}. (c) Velocity contour diagrams of Kr photofragments similar to the one in Figure 2B, with the intensity multiplied by a factor of 15.

TABLE 2: Kr_2 Transitions near the Kr $^1S_0$ + Kr (5p)[1/2]$_0$ Dissociation Limit

v''	v'	two-photon energy (cm^{-1})	$\Delta G'$ (cm^{-1})	Dehmer and Pratt, ref 19
0	0	93 841	48.8	93 838.4
0	1	93 890	46.2	93 890.6
0	2	93 936	42.2	93 937.6
0	3	93 979	41.8	93 984.1
0	4	94 020	38.0	94 024.1
0	5	94 058		not obsd

displacement of the ions from the center of the image to the speed of these fragments. Because both concomitant fragment masses are known (assuming, for simplicity, a mass of 84 amu for Kr), the measured speed can be converted to total fragment kinetic energy (the total kinetic energy is just $m_{Kr}v_{Kr}^2$). In Figure 3B the Kr photofragment intensities are plotted versus the total fragment kinetic energy. The kinetic energy release for the inner channel peaks at 0 eV and is approximately 0.2 eV broad, whereas the kinetic energy release for the outer channel peaks at approximately 4.9 $\pm$ 0.1 eV. The angular distribution of the Kr^+ ions in the outer ring is shown in Figure 3C and reveals that the fragments in the outer channel recoil primarily parallel to the laser polarization vector. The solid line in Figure 3C is the calculated angular distribution for a dissociation described by a single anisotropy parameter, $\beta_2 = 2$. Kr photofragment ion images obtained for the other vibrational bands of this electronic band are approximately identical.

Also Kr photofragment ion images obtained at transitions from other electronic bands are essentially identical to the image shown in Figure 2A. Branching ratios between the inner and outer channels of all measured images are given in Table 3. Additionally, the assignments of these transitions as given by Lipson et al.[23] are shown in Table 3.

ArKr. ArKr molecules were prepared in a 10:1 mixture of argon and krypton. Even in such a mixture the resonant ion signals for Kr_2 dimers are a factor of 5 higher than those observed for the ArKr molecules. Transitions attributed to these two different molecules can be separated easily via mass selective detection of the ions. No transitions producing Ar_2^+ ions are observed. This absence was expected because no gerade states of Ar_2 are energetically accessible in the studied energy region (the lowest lying excited gerade state of Ar_2 is above 96 000 cm^{-1} [9]). In Figure 4 part of the (2+1) REMPI spectrum of ArKr in the region of the Ar $^1S_0$ + Kr (5p) [1/2]$_0$ and Kr $^1S_0$ + Ar (4s) $[3/2]^\circ_1$ dissociation limits is shown; REMPI spectra of $ArKr^+$, Ar^+, and Kr^+ are displayed. Note that $ArKr^+$ signals are accompanied by Ar^+ signals but not by Kr^+ signals. Kr^+ signals observed in this energy region coincide with Kr_2^+ signals and belong to Kr_2 resonances listed in Table 2. Two electronic bands of ArKr are observed; the vibronic transitions are listed in Table 4. Our transitions are the same as those reported by Dehmer and Pratt.[19] The electronic band starting at 93 699 cm^{-1} consists of three vibrational transitions, separated by approximately 70 cm^{-1}. The electronic band starting at 94 180 cm^{-1} consists of two vibrational transitions, separated by approximately 43 cm^{-1}. All five observed ArKr transitions lead to the production of $ArKr^+$ and Ar^+ signals but not to Kr^+ signals.

The Band Starting at 93 699 cm^{-1}. The electronic band starting at 93 699 cm^{-1} consists of three two-photon transitions. In Figure 5A an ion image of the Ar photofragments is shown taken with the laser wavelength tuned to the 93 844 cm^{-1} ArKr resonance. Ar photofragment ion images taken at the other two transitions of this electronic band are qualitatively identical. In Figure 5B the velocity contour plot obtained from this image is shown. The image and velocity contour plots show two channels that are both anisotropic. The contributions of the outer and inner channels to the image are 92% and 8%, respectively. In Figure 6A a plot is shown of the intensity distribution along a single column of the CCD, through the center of the image. In Figure 6B the Ar photofragment distribution is plotted versus the total fragment kinetic energy. Figure 6B shows that the kinetic energy release for the inner channel peaks at 90 $\pm$ 50 meV, whereas the outer channel peaks at 3.8 $\pm$ 0.1 eV. In Figure 6C the angular distribution of the Ar fragments in the outer ring is shown. The angular distribution of the fragments in the outer channel can be described by a distribution that is nearly $\cos^2\theta$ with respect to the laser polarization vector. The solid line in Figure 6C is the angular distribution for a dissociation described by a single anisotropy parameter, $\beta_2 = 2$. Branching ratios for the inner and outer channels in the Ar photofragment ion images measured at the vibrational transitions of this electronic band are given in Table 5.

The Band Starting at 94 180 cm^{-1}. The electronic band starting at 94 180 cm^{-1} consists of a pair of two-photon transitions. Ar photofragment ion images at both these transitions are qualitatively identical. An image and the velocity contour plot of the Ar^+ photofragments at the 94 180.0 cm^{-1} resonance are shown in Figure 5, C and D, respectively. The image and velocity contour plot show two channels that are both anisotropic. The contribution of the two channels to the image is 19% and 81% for the outer and inner channel, respectively. In Figure 7A a plot is shown of the intensity distribution along a single column of the CCD, through the center of the image, and in Figure 7B the Ar photofragment distribution is plotted

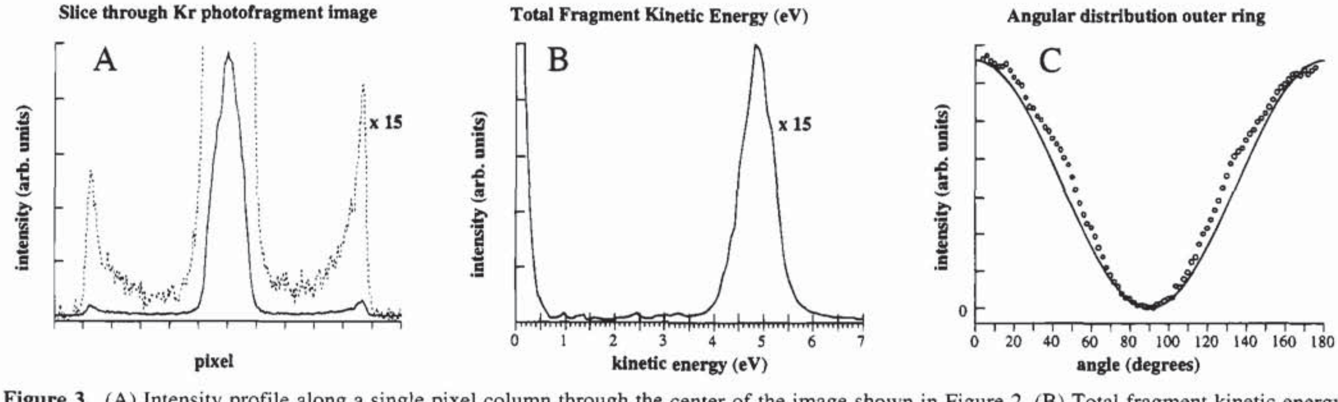

Figure 3. (A) Intensity profile along a single pixel column through the center of the image shown in Figure 2. (B) Total fragment kinetic energy release distribution for the image shown in Figure 2A. (C) Angular distribution of Kr photofragments in the outer ring of the image shown in Figure 2A. The solid line represents an angular distribution corresponding to a $\beta_2 = 2$ anisotropy parameter.

TABLE 3: Contributions of the Inner and Outer Channel in the Kr Photofragment Ion Images

two-photon energy (cm^{-1})	inner channel (%)	outer channel (%)	assignment[23]	$v''-v'$
	Kr $^1S_0$ + Kr (5p)$[1/2]_0$ Dissociation Limit			
93 841	77	23	$0_g^- \to 0_g^-$	$0 \to 0$
93 890	75	25	$0_g^- \to 0_g^-$	$0 \to 1$
93 936	85	15	$0_g^- \to 0_g^-$	$0 \to 2$
93 979	78	22	$0_g^- \to 0_g^-$	$0 \to 3$
94 020	72	28	$0_g^- \to 0_g^-$	$0 \to 4$
	Kr $^1S_0$ + Kr (5p)$[3/2]_2$ Dissociation Limit			
93 142	61	39	$0_g^+ \to 0_g^+$	$0 \to 0$
93 153	60	40	$0_g^+ \to 0_g^+$	$0 \to 1$
	Kr $^1S_0$ + Kr (5p)$[5/2]_2$ or (5p)$[5/2]_3$ Dissociation Limit			
92 215	61	39	$0_g^- \to 2_g$	$0 \to 0$
92 122	60	40	$0_g^- \to 1_g$	$0 \to 4$

versus the total fragment kinetic energy. The plot in Figure 7B shows that the kinetic energy release for the inner channel peaks at 120 ± 50 meV, the outer channel peaks at 3.9 ± 0.1 eV. In Figure 7C the angular distribution of the Ar^+ ions in the outer ring is shown. The solid line in Figure 7C is the angular distribution for a dissociation described by a single anisotropy parameter, $\beta_2 = 2$. It can be seen that the angular distribution of the fragments in the outer channel has a distribution that is nearly $\cos^2 \theta$ with respect to the laser polarization vector. Branching ratios for the inner and outer channels in the Ar photofragment ion images measured at the vibrational transitions of this electronic band are given in Table 5.

Discussion

Using the photofragment ion imaging technique, we have studied several two-photon-excited states of Kr_2 and ArKr, whose transition frequencies were reported previously.[19,20,23] Our photofragment ion imaging studies of Kr_2 and ArKr reveal in detail the dissociation and ionization dynamics of the two-photon resonantly excited states. Additionally, our study enables us to reassign transitions observed for the ArKr molecule to transitions in which the Ar moiety is excited.

Kr_2. For Kr_2, we examined the dissociation and ionization dynamics of electronic states spectroscopically characterized previously by Echt et al.,[20] Dehmer and Pratt,[19] and Lipson et al.[23] Additional spectroscopic information on Kr_2 gerade states in this spectral region is available from the transient absorption studies of Eden and co-workers.[25,26,28] However, the intermediate metastable triplet state used by Eden and co-workers has an equilibrium bond length of only 2.21 Å[12] (compared with 4.02 Å for the ground state[12]), and the parts of the excited state potential energy surfaces they probe are at different geometries than those probed in our study. Therefore, transitions observed in our (2+1) REMPI study are not easily correlated to transitions observed in their transient absorption studies.

On the basis of theoretical calculations[8] the transitions we observe in the region of the Kr $^1S_0$ + Kr (5p)$[1/2]_0$ dissociation limit (see Table 2) are attributed to excitation to the 0_g^- (5p)$[1/2]_0$ molecular state, which is predicted to have two minima.[8] This state is also the only molecular state that correlates to the Kr $^1S_0$ + Kr (5p)$[1/2]_0$ atomic asymptotes. The outer minimum has a calculated r_e of 3.6 Å, a dissociation energy of 152 cm^{-1}, and a ω_e of 63 cm^{-1} (close to the observed vibrational spacing). The inner minimum of this state has a r_e of 2.8 Å and is too high in energy to be accessed. The Kr_2 transitions we observe in the region of the Kr $^1S_0$ + Kr (5p)-$[3/2]_2$ dissociation limit are attributed to excitations to the 0_g^+

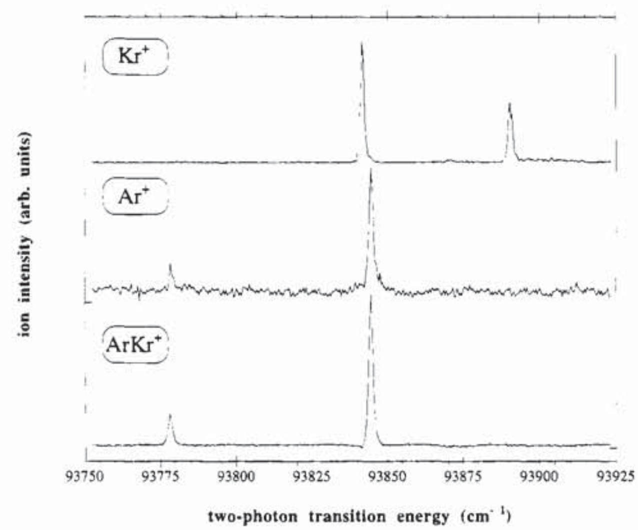

Figure 4. Two-photon resonant ionization spectrum of ArKr, Ar, and Kr in the energy region near the Kr* (5p) $[1/2]_0$ state. Ionization signals of ArKr and Ar are observed at the same two-photon energies, whereas ionization signals of Kr are observed only at Kr_2 two-photon resonances.

TABLE 4: ArKr Transitions near the Ar $^1S_0$ + Kr (5p) $[1/2]_0$ and Kr $^1S_0$ + Ar (4s) $[3/2]_1$ Dissociation Limits

v''	v'	two-photon energy (cm^{-1})	$\Delta G'$	Dehmer and Pratt, ref 19 (two-photon)	Tanaka et al., ref 10 (one-photon)
0	$m+0$	93 699	75.8	93 696.5	not observed
0	$m+1$	93 775	68.5	93 772.3	
0	$m+2$	93 844		93 841.1	
1	0				94 158.4
0	0	94 180	43.4	94 177.9	94 180.5
1	1				94 201.8
0	1	94 223		94 221.2	

(5p)$[3/2]_2$ state, which is only weakly bound, but has a minimum at approximately the same r_e value as the ground state.[8] Unambiguous assignment of the other bands is more complicated because the asymptotic atomic states give rise to several molecular states found in the same energy region.[8] A discussion of possible assignments has appeared elsewhere.[8,19,20,23]

Our data reveal that, at the laser fluences used, two-photon absorption to the above mentioned gerade intermediate states is followed by several processes. Some of the following processes can be expected:

dimer ionization

$$Kr_2^* \xrightarrow{h\nu} Kr_2^+ + e^- \quad (1)$$

dissociative ionization

$$Kr_2^* \xrightarrow{h\nu} Kr^+ + Kr + e^- \quad (2)$$

predissociation, followed by excited fragment ionization

$$Kr_2^* \to Kr^* + Kr \xrightarrow{h\nu} Kr^+ + Kr + e^- \quad (3)$$

three-photon absorption, followed by dimer dissociation and excited fragment ionization

$$Kr_2^* \xrightarrow{h\nu} Kr_2^{**} \to Kr^* + Kr \xrightarrow{h\nu} Kr^+ + Kr + e^- \quad (4)$$

in which $\Rightarrow$ indicates a photon absorption and $\to$ a dissociation. The contribution of process 1 is evident from the observation

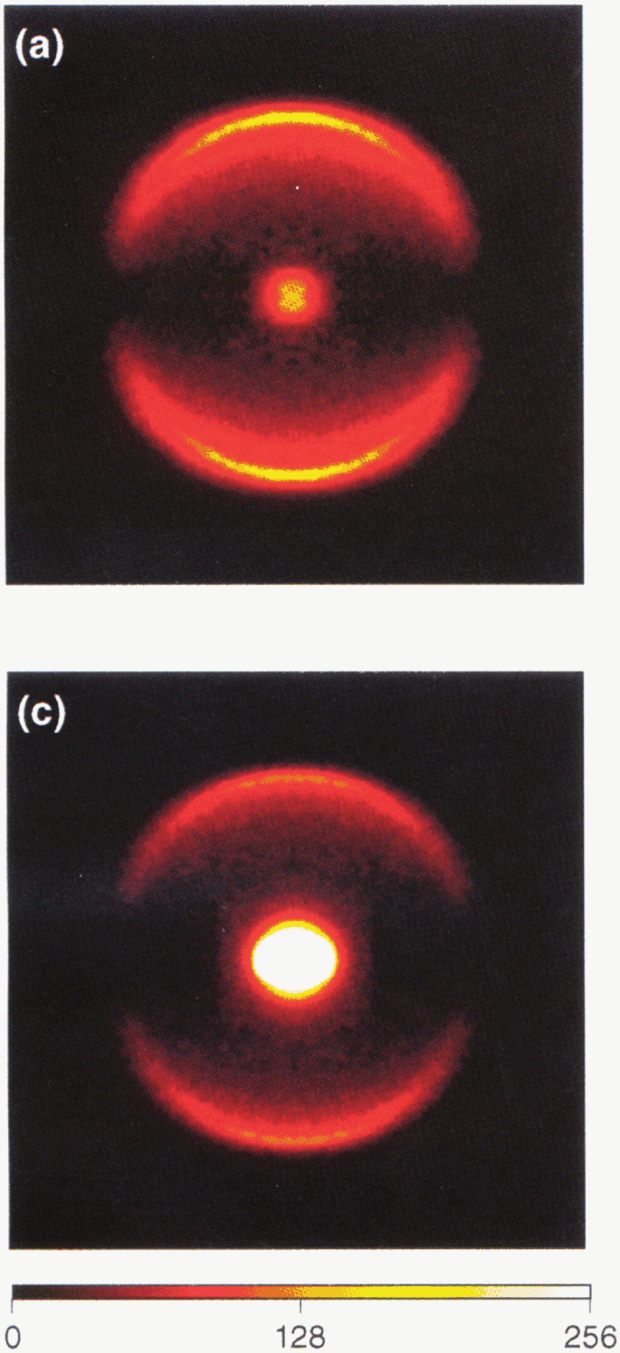

Figure 5. (A) Photofragment ion image of Ar, taken with the laser frequency tuned to a two-photon resonance of the ArKr molecule at 93 844 cm^{-1}. (B) Velocity contour diagram of the Ar photofragments after resonant two-photon excitation at 93 844 cm^{-1}. (C) Photofragment ion image of Ar, taken with the laser frequency tuned to a two-photon resonance of the ArKr molecule at 94 180 cm^{-1}. (D) Velocity contour diagram of the Ar photofragments after resonant two-photon excitation at 94 180 cm^{-1}.

of the dimer ion signal in the REMPI scans. The one-photon energy is approximately 5.6 eV; therefore, a subsequent photon is sufficient to bring the two-photon-excited intermediate states above the dimer ionization limit, which is 12.87 eV.[38] Because the dissociation energy of the Kr_2^+ ion is 1.15 eV, dissociative ionization (process 2) is also energetically allowed after absorption of three photons. The intermediate state at the two-photon level may predissociate (process 3), a process that has been observed previously for two-photon-excited KrXe[17] and Xe_2[39] using REMPI-PES. This predissociation leads to a ground state and an excited state Kr fragment. The lowest excited state of Kr (the $5s[3/2]_2$, $^3P_2$ state) is situated 9.9 eV above the ground state. A third UV photon is, therefore, sufficient to ionize excited state Kr fragments. In contrast to the first three processes, process 4 is a four-photon process. In this process, the intermediate state at the two-photon level absorbs a third photon to a dissociative state (or continuum) above the ionization limit of the Kr_2 molecule. Dissociation of this three-photon-excited state results in a ground state and an excited state Kr fragment. As in process 3, a subsequent photon may ionize the excited state fragments.

The image of the Kr photofragments, shown in Figure 2A, was taken with the laser frequency at a two-photon resonance of the dimer at 93 890 cm^{-1}. Two velocity sets of Kr fragments are formed. The angular distribution of the slower photofragments at the center of the image appears isotropic; $\beta_2 = 0$. These Kr photofragments are excited state fragments formed via predissociation of the two-photon intermediate (process 3). The

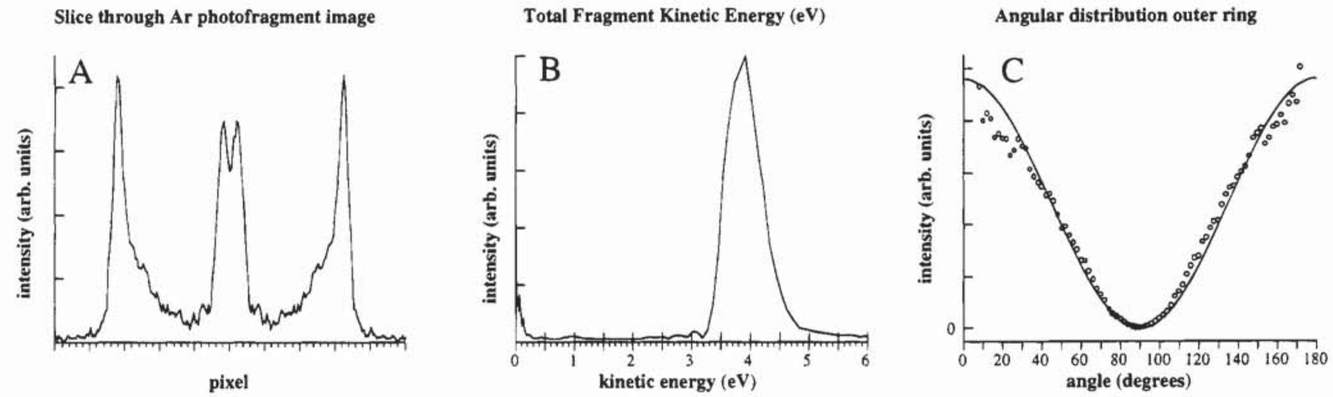

Figure 6. (A) Intensity profile along a single pixel column through the center of the image shown in Figure 5A. (B) Total fragment kinetic energy release distribution for the image shown in Figure 5A. (C) Angular distribution of Ar photofragments in the outer ring of the image shown in Figure 5A. The solid line represents an angular distribution corresponding to a $\beta_2 = 2$ anisotropy parameter.

TABLE 5: Contributions of the Inner and Outer Channel in the Ar Photofragment Ion Images

two-photon energy (cm^{-1})	inner channel (%)	outer channel (%)
93 699	9	91
93 775	9	91
93 844	8	92
94 180	81	19
94 223	86	14

calculations of Audouard et al.[8] predict that the 0_g^+ (5p)[1/2]$_0$ state has a dissociation energy of only 152 cm^{-1}. The predissociation leads initially to Kr (5p) excited state fragments, of which several are energetically accessible ($^3S_1$, $^3D_3$, $^3D_2$, $^3D_1$, and $^1D_2$; see Table 1). The energy separation between these 5p states is less than 2000 cm^{-1}. Therefore, predissociation into several excited states may contribute to the signal observed at the center of the image. Unfortunately, contributions from various (5p state) predissociation channels cannot be resolved in our study. Initially formed 5p excited states may fluoresce to lower 5s states. The lifetime of the Kr (5p) states averages 25−40 ns.[40−42] Although fluorescence will change the branching ratios observed in the images, fluorescence will not change the kinetic energy of the fragments. We observe no direct predissociation into Kr (5s) states, as fragmentation to Kr $^1S_0$ + Kr (5s) will be accompanied by a kinetic energy release of 1.0 eV (Kr $^1P_1$) to 1.7 eV (Kr $^3P_2$). No such fragments are observed in the Kr photofragment ion images.

Comparison of our photofragment ion imaging results for the Kr_2 predissociation with the REMPI-PES data of Dehmer and Pratt[19] is interesting. Dehmer and Pratt recorded a photoelectron spectrum after two-photon excitation to the $v' = 1$ band at 93 890 cm^{-1}. This PES spectrum reveals not only that various excited states of the Kr_2^+ are formed but also the predissociation of the two-photon level (0_g^+ (5p)[1/2]$_0$). The PES spectrum has sufficient resolution to reveal the branching ratios for the various Kr 5p states formed. Dehmer and Pratt concluded that Kr (5p)[3/2]$_{2,1}$ was predominantly formed in the predissociation and much less Kr (5p)[5/2]$_{2,3}$ and Kr (5p)[1/2]$_1$. Our photofragment ion imaging study confirms the significance of predissociation, but it does not reveal which Kr (5p) states are populated.

Three-photon absorption excites the molecule to states with approximately 17.5 eV of internal energy. Formation of the $^2P_{3/2}$ and $^2P_{1/2}$ Kr^+ ionic states requires 14.0 and 14.6 eV, respectively. Thus, dissociative ionization is energetically accessible. Conservation of energy dictates that the ionic Kr^+ fragments will be formed with a total fragment kinetic energy less than 3.5 or 2.9 eV for the two ionic states, respectively. The absence of ions with these kinetic energies indicates that dissociative ionization processes are not very significant under our experimental conditions. An alternative channel could be absorption of a photon by one of the excited states of the Kr_2^+ dimer ion, which subsequently dissociates into Kr^+ and Kr $^1S_0$. Absorption of a 5.8 eV photon by the dimer ion allows access to several dissociative states of the ion, which correlate to Kr^+ $^2P_{3/2}$ + Kr $^1S_0$ and $^2P_{1/2}$ Kr^+ + Kr $^1S_0$ asymptotes. Therefore, we expect that such a process will most probably lead to Kr^+ $^2P_{3/2}$ as well as $^2P_{1/2}$ Kr^+ ions, which we would observe as separate rings in the images. Since the PES data of Dehmer and Pratt indicate that several excited states of the ion are populated, we expect that dissociation via this mechanism would produce many different rings in the images. Dehmer and Pratt find that Kr_2^+ ions are predominantly formed in the B $^2\Pi_{3/2\ g}$, and C $^2\Pi_{3/2\ g}$ states. When these ions subsequently absorb a photon and dissociate into Kr^+ $^2P_{3/2}$ + Kr $^1S_0$, the fragments will be formed with a total fragment kinetic energy release of 5.7 and 5.8 eV, respectively. In all of the Kr photofragment images, measured at different excitation energies, we observe a single outer ring, with a speed that does not agree with any of these mechanisms. Therefore, we conclude that such processes are not important under our experimental conditions.

Instead, fragments with a total kinetic energy release of approximately 4.9 eV are observed. Assuming that dissociation occurs after three-photon absorption, the internal energy of the Kr atomic fragments formed via process 4 is given by

$$E_{\mathrm{internal}}(\mathrm{Kr}^*) + E_{\mathrm{internal}}(\mathrm{Kr}\ ^1S^0) = E_{\mathrm{internal}}(\mathrm{Kr}^*) = 3h\nu - \mathrm{TKE} \quad (5)$$

where $h\nu$ is the one-photon energy and TKE is the measured total fragment kinetic energy. In Figure 8 a plot of the distribution of the fragments in the outer ring of the image versus the internal energy of the Kr* atoms is shown. It reveals that the internal energy of the Kr atoms observed in the outer ring of the image is approximately 12.6 eV. The width of this peak is 0.7 eV (fwhm). This observed width of the Kr^+ outer ring is resolution limited, and therefore, we cannot determine whether several Kr excited atomic states contribute to this signal. Some of the possible Kr* excited states are indicated in Figure 8. Between 12.2 and 13.0 eV are several 4d, 5p, 5d, 6s, and 6p states.[43] The images reveal that three-photon absorption, which brings the molecule far above the ionization limit, leads to dissociation into neutral products, not ionic products.

Because Dehmer and Pratt[19] did not measure photofragment velocities, they were unable to determine whether three-photon absorption processes were important in their study. They used

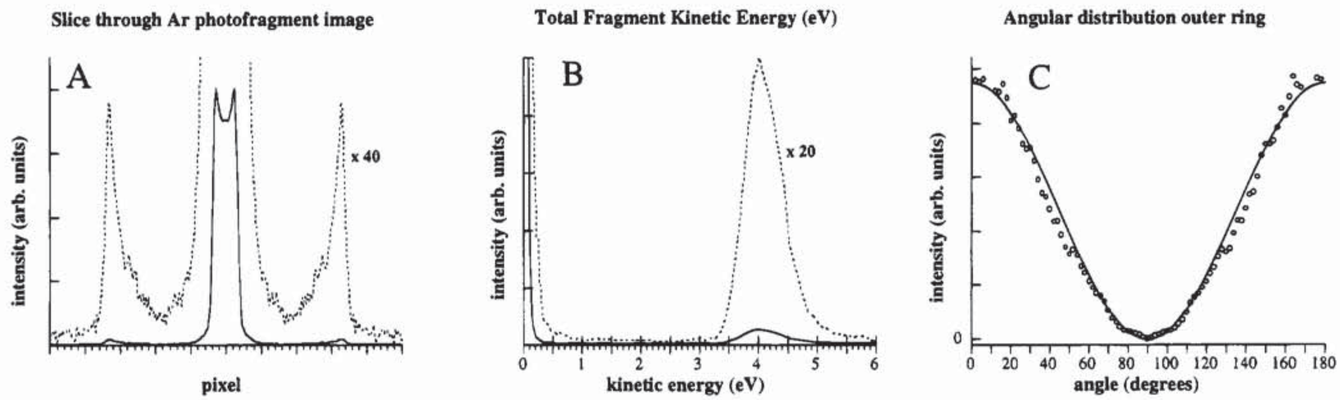

Figure 7. (A) Intensity profile along a single pixel column through the center of the image shown in Figure 5C. (B) Total fragment kinetic energy release distribution for the image shown in Figure 5C. (C) Angular distribution of Ar photofragments in the outer ring of the image shown in Figure 5C. The solid line represents an angular distribution corresponding to a $\beta_2 = 2$ anisotropy parameter.

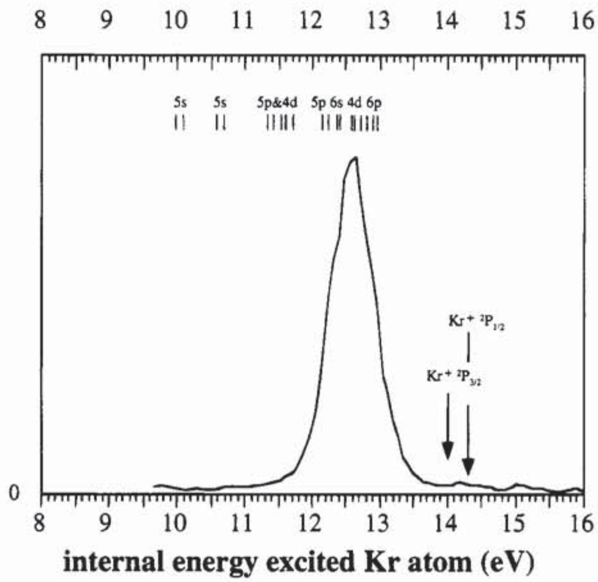

Figure 8. Internal energy of the excited Kr atoms formed in the outer ring of the image shown in Figure 2A. The comb at the top indicates Kr atomic energies; the arrows indicate expected energies corresponding with formation of ground and spin–orbit excited states of the Kr^+ ion.

laser fluences that were a factor of 10 smaller than we used (50 and 500 μJ, respectively), which decreased the importance of higher order processes in their study. Knowing from our work that excited states of Kr are formed with approximately 12.6 eV internal energy, we note that the kinetic energies of electrons formed via process 4 would be 4.4 eV (corresponding with formation of Kr^+ $^2P_{3/2}$) and 3.8 eV (corresponding with formation of Kr^+ $^2P_{1/2}$). Dehmer and Pratt observed photoelectron signals that correspond to electrons with kinetic energies of approximately 3.9 eV (which were not assigned), but they did not observe a significant amount of electrons with kinetic energies of approximately 4.4 eV.

The angular distribution of the Kr photofragments formed after three-photon absorption by the Kr_2 dimer is modeled quite well by a single anisotropy parameter, $\beta_2 = 2$. This $\cos^2\theta$ angular distribution indicates that the dissociation at the three-photon level is reasonably fast, and the Kr photofragments recoil primarily along the laser polarization vector. Angular distributions of photofragments after multiphoton absorption processes depend on the symmetries of the electronic states involved (real or virtual) and on the lifetimes of the intermediate states.[44-47] Angular distribution functions of photofragments after a two-photon absorption have been derived by Zare[44] and Sander and Wilson.[45] Similarly, and in accord with the symmetry considerations given by Yang,[48] the angular distribution of photofragments following a three-photon absorption process, $I(\theta)$, can, in general, be modeled by

$$I(\theta) \approx 1 + \beta_2 P_2(\cos\theta) + \beta_4 P_4(\cos\theta) + \beta_6 P_6(\cos\theta) \qquad (6)$$

where $P_m(\cos\theta)$ is the mth order Legendre polynomial and β_m are the anisotropy parameters. Using eq 6, a best fit to the angular distribution of the Kr photofragments in the outer ring of the image shown in Figure 2A is obtained with the parameters $\beta_2 = 1.85$, $\beta_4 = -0.25$, and $\beta_6 = 0$; that is, the higher order terms are quite small. From our experimental data it is difficult to separate the effect of each step in the multiphoton process on the observed angular distributions. However, the fact that the observed Kr photofragment angular distribution, after three-photon absorption, can be described quite well by a single $\cos^2\theta$ angular distribution (neglecting the small higher order terms) indicates that part of the $\mu - v$ correlation cancels out. Similar behavior was observed previously following two-photon absorption processes.[47,49] The center channel in the Kr photofragment ion images appears to be isotropic. Therefore, the observed $\cos^2\theta$ angular distribution of the Kr photofragments in the outer channel may originate from the absorption of the third photon in a parallel transition.

On the basis of theoretical calculations[8] the transitions observed in the region of the Kr $^1S_0$ + Kr (5p)[1/2]$_0$ dissociation limit (see Table 2) are attributed to excitation from the ground state to the 0_g^+ (5p)[1/2]$_0$ state. We have discussed our Kr photofragment ion imaging results for excitation to this two-photon resonant state in detail, because they can be compared with the REMPI-PES data of Dehmer and Pratt.[19] The other Kr_2 electronic transitions we studied exhibit similar dynamics. Besides ionization of the dimer (process 1), resonant excitation of Kr_2 generally leads to extensive predissociation at the two-photon level: to Kr $^1S_0$ + Kr* (process 2). Additionally, three-photon absorption processes are observed, which access dissociative excited states far above the Kr_2 ionization limit. These neutral states dissociate rapidly into Kr $^1S_0$ + Kr* in 4d, 5p, 5d, 6s, and/or 6p atomic states (process 4). For all studied electronic transitions the angular distributions of the Kr photofragments formed following three-photon absorption can be modeled by a pure $\cos^2\theta$ distribution. Dissociative ionization is not observed. The relative contributions of the inner and outer channel to the Kr photofragment ion images is likely to be laser-power dependent. Because all Kr photofragment ion images were taken under identical conditions, the observed differences in the relative contributions from the inner and outer channels indicate the relative importance of processes 2 (predissociation) and 4 (three-photon absorption, followed by dissociation into neutral fragments) at the experimental laser fluence.

ArKr. We have examined the dissociation and ionization dynamics of electronic states of ArKr in the same spectral region studied by Dehmer and Pratt.[19] Tanaka et al.[10] examined the spectrum of ArKr produced in a bulb at 160−180 K in the same energy region using one-photon absorption spectroscopy. They observed three transitions, at 94 158.4, 94 180.5 (the most intense band), and 94 201.8 cm^{-1}. The transitions observed by Tanaka et al. may belong to the same electronic band that we observe (starting at 94 180 cm^{-1}). As suggested by Dehmer and Pratt, the two weaker additional features Tanaka observed may represent hotbands, originating from the first vibrationally excited level of the ground state. This assignment leads to a vibrational spacing of 22 cm^{-1} in the ground state, which is in good agreement with a theoretical value of 23.65 cm^{-1}.[50] If we assume that the one-photon transitions observed by Tanaka et al. belong to the same electronic band system as the two-photon transitions we observe, the excited state must have an electronic symmetry that allows one-photon and two-photon excitation from the ground state. One- and two-photon dipole allowed transitions from the 0^+ ArKr ground state are transitions to states with $\Omega = 0^+$ or 1. Tanaka et al.[10] did not observe transitions in the energy region of the electronic band we observe starting at 93 699 cm^{-1}, which indicates that transitions to this electronic state are two-photon allowed, but not one-photon allowed. We therefore conclude that the ArKr electronic excited state corresponding with these transitions is an $\Omega = 2$ state.

Tanaka et al.[10] and Dehmer and Pratt[19] attributed the band starting at 94 180 cm^{-1} to transitions to an ArKr excited state, in which the excitation takes place on the Kr moiety that correlates to the Ar $^1S_0$ + Kr (5p)$[1/2]_0$ atomic products. This tentative assignment was made because the observed transitions are close to the transition to the Kr (5p)$[1/2]_0$ atomic level and because they are similar to resonances observed for Kr_2 in the same energy region (see above). The band starting at 93 699 cm^{-1} was not assigned. We observe that resonant two-photon absorption in ArKr is followed by ionization to give $ArKr^+$ and by formation of Ar^+ ions, but not Kr^- ions. This behavior would be rather unexpected if the initial two-photon excitation takes place at the Kr moiety of the molecule. Electronic energy transfer,

$$ArKr^* \Leftrightarrow Ar^*Kr \qquad (7)$$

from the Kr to the Ar moiety within the molecule is possible. Setser and co-workers[41,51] observed electronic energy transfer between Ar (4s) $[3/2]^\circ_2$ and Kr $^1S_0$ (and *vice versa* from Kr (5p) to Ar) in bimolecular collisions. They measured state-to-state rate constants for these processes, which were on the order of approximately 5×10^{-12} $molecule^{-1}$ cm^3 s^{-1}, more than an order of magnitude lower than the collision rate. Electronic energy transfer is thus not very efficient in this system. For example, Setser and co-workers observed that Ar (4s) $[3/2]^\circ_2$ transfers electronic energy state-selectively to Kr (5p)$[3/2]_2$ and Kr (5p)$[3/2]_1$, but not to any other Kr 5p or 5s level. Conversely, Kr (5p) excited states transfer electronic energy to Ar (4s) $[3/2]^\circ_2$ at similar rates. Assuming initial Kr excitation ($ArKr^*$), the observed exclusive formation of Ar^+ ions would indicate complete electronic energy transfer to the Ar moiety within the time window of the laser pulse (≈5 ns). Such complete electronic energy transfer is not very likely. Therefore, we conclude that the transitions we observe for the band starting at 93 699 cm^{-1} and the band starting at 94 180 cm^{-1} are excitations to states of the ArKr molecule in which the Ar moiety is excited (Ar*Kr).

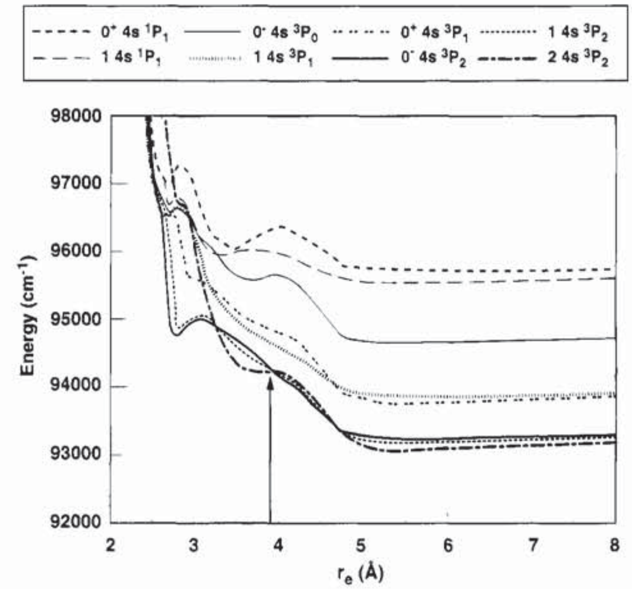

Figure 9. Potential energy curves of ArKr excited states that correlate with Ar (4s) − Kr $^1S_0$ asymptotes. Curves are adapted from ref 7. The arrow coincides with r_e in the ArKr ground state.

This assignment is supported by recently calculated *ab initio* potential energy curves of ArKr.[7] In the energy range studied in our work several Ar*-excited ArKr states are calculated that correlate to Ar* (4s) + Kr $^1S_0$; the corresponding potential energy curves are shown in Figure 9. All these Ar*Kr states are repulsive or quasi-bound, which is in contrast with homonuclear Ar_2[14] and Kr_2[12] dimers, for which some of the lower *n*s excited states are strongly bound (by as much as 6000 cm^{-1}). Kr (5s)-excited ArKr* states are also calculated to be quasi-bound or repulsive.[7] As mentioned in the Introduction, this remarkable difference in bonding characteristics arises from the stronger interaction in homonuclear dimers (degenerate atomic orbitals) than in heteronuclear dimers (nondegenerate atomic orbitals).

Both observed electronic bands are close in energy to the Ar (4s) $[3/2]^\circ_1$ + Kr $^1S_0$ atomic dissociation limit. Figure 9 shows, however, that excited states that correlate with this Ar (4s) $[3/2]^\circ_1$ + Kr $^1S_0$ dissociation limit cannot be accessed, assuming vertical transitions from the ground state (r_e = 3.9 Å) at the two-photon energies we used. Only Ar*-excited states that correlate to the Ar (4s) $[3/2]^\circ_2$ + Kr $^1S_0$ atomic asymptotes can be accessed at these two-photon energies. These three electronic states are states with $\Omega = 0^-$, 1, and 2. Transitions to the $\Omega = 0^-$ state are two-photon forbidden. We conclude, therefore, that the observed electronic bands correspond to excitations to the Ω = 1 or 2 states that correlate to the Ar (4s) $[3/2]^\circ_2$ + Kr $^1S_0$ dissociation limit. Quasi-bound minima have been calculated for both the Ω = 1 and 2 states at internuclear distances near that of the ground state (see Figure 9). As mentioned above, our electronic band starting at 94 180 cm^{-1} was also observed by Tanaka et al.[10] as a one-photon absorption; we therefore assign it to the Ω = 1 state. Because no one-photon absorption signals were found by Tanaka et al.[10] at energies near the electronic band starting at 93 699 cm^{-1}, we conclude that this band corresponds with the Ω = 2 state.

The REMPI and ion-imaging data reveal that at the laser fluences used the two-photon absorption is followed by several processes. As with Kr_2 we are led to expect some of the following processes:

ArKr ionization

$$\mathrm{Ar^*Kr} \xrightarrow{h\nu} \mathrm{ArKr^+} + \mathrm{e^-} \tag{8}$$

dissociative ionization

$$\mathrm{Ar^*Kr} \xrightarrow{h\nu} \mathrm{Ar^+} + \mathrm{Kr} + \mathrm{e^-} \tag{9}$$

predissociation, followed by excited fragment ionization

$$\mathrm{ArKr^*} \rightarrow \mathrm{Ar^*} + \mathrm{Kr} \xrightarrow{h\nu} \mathrm{Ar^+} + \mathrm{Kr} + \mathrm{e^-} \tag{10}$$

three-photon absorption, followed by ArKr dissociation and excited fragment ionization

$$\mathrm{ArKr^*} \xrightarrow{h\nu} \mathrm{ArKr^{**}} \rightarrow \mathrm{Ar^*} + \mathrm{Kr} \xrightarrow{h\nu} \mathrm{Ar^+} + \mathrm{Kr} + \mathrm{e^-} \tag{11}$$

in which ➡ indicates photon absorption and → dissociation. Process 8 is evident from the observation of $ArKr^+$ signals in the REMPI scans. Absorption of three photons is sufficient to bring the two-photon-excited intermediates above the ArKr ionization limit (13.5 eV[31,32]). Because the dissociation energy of the $ArKr^+$ ion is only 0.5 eV, dissociative ionization (process 9) is energetically accessible after absorption of three photons. Dissociative ionization into Kr^+ + Ar products is energetically more favorable than dissociation into Ar^+ + Kr (by 1.76 eV). The REMPI data show, however, that processes leading to the formation of Kr^+ ions are not very significant. Predissociation, process 10, might lead to Kr $^1S_0$ + Ar $^3P_2$ excited state fragments. Calculations by Spiegelmann et al.[7] (see Figure 9) reveal that both the $\Omega = 1$ and 2 states are crossed by the two-photon-forbidden $\Omega = 0^-$ state, which may play a role in the observed predissociation. Predissociation to Kr $^1S_0$ + Ar $^3P_2$ fragments will be accompanied by a total kinetic energy release of approximately 80 and 125 meV, for excitation to the bands starting at 93 699 and 94 180 cm^{-1}, respectively. These calculated total kinetic energy releases are consistent with the experimentally observed energy releases of the inner ring in the images.

The internal energies of the excited state Ar fragments can be deduced from the images using a strategy similar to that outlined in eq 5. In Figure 10 the distribution of the Ar photofragments in the outer ring of the image versus the internal energy of the Ar* atoms is plotted. This plot reveals that the internal energies of the Ar atoms, observed in the outer ring of the images for both observed electronic bands, are approximately 13.3 eV (assuming absorption of three photons). The observed width is resolution-limited and is for both rings approximately 0.7 eV (fwmh). Some of the possible Ar* excited states formed are indicated in Figure 10. Several Ar (4p) states are located between 12.6 and 14.0 eV,[52] but we are not able to resolve which states are formed. The images do reveal, however, that other Ar excited states, such as 4s, 5s, 3d, and 5p, are not formed. Additionally, the images and Figure 10 show that three-photon absorption leads to dissociation into neutral fragments (process 11), not directly to ionic products (process 9).

The ion images obtained for the two electronic ArKr states investigated are somewhat similar but also remarkably different. The two electronic states exhibit similar dynamics: direct ionization of the two-photon resonant levels (process 8) competes with predissociation of the two-photon resonant level (process 10) and with three-photon absorption, followed by dissociation into neutral fragments (process 11). The images directly reveal the competition between the latter two processes. The ion images taken for transitions to the band starting at 93 699 cm^{-1}, which is an excitation to the $\Omega = 2$ state, display approximately a factor of 10 more signal in the outer ring than in the inner ring. The images taken for transitions to the band starting at 94 180 cm^{-1}, which is an excitation to a $\Omega = 1$ state, display approximately a factor of 5 less signal in the outer ring than in the inner ring. Our experiments reveal the competition between these different processes in the time window of the laser pulse (≈5 ns). It is expected that the ratio of the two channels depends on the laser fluences used, but this laser fluence is kept constant for all recorded images. The marked difference between the images taken for the two electronic bands can have several additional sources. First, the cross section for absorption of a third photon may be different for the two-photon intermediate states. Three-photon absorption leads to approximately 17.5 eV of excitation energy in the ArKr molecule. The number and electronic symmetries of excited states in this energy region are unknown. Enhanced absorption by resonant effects, leading to markedly different cross sections, might influence the competition between predissociation (process 10) and three-photon absorption processes (process 11). Second, and more likely, the predissociation rates of the two-photon resonant excited $\Omega = 1$ and 2 states may be different. The predissociation rates are determined by the depths of the wells and/or barriers to dissociation of the quasi-bound states and by the interaction with the $\Omega = 0^-$ state, which crosses both the $\Omega = 1$ and 2 states.[7] Calculations[7] show that the local minimum of the $\Omega = 2$ state is a little deeper than that of the $\Omega = 1$ state, in agreement with the slower predissociation rate observed for the $\Omega = 2$ state.

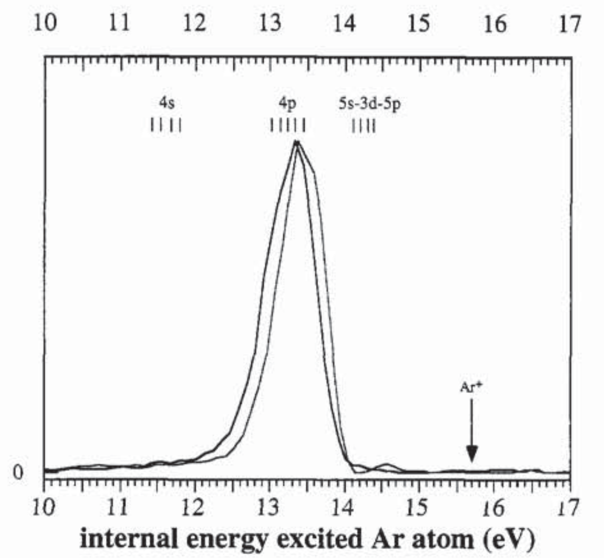

Figure 10. Internal energy of the excited Ar atoms formed in the outer ring of the image shown in Figure 5A (gray) and 5C (black). The comb at the top indicates Ar atomic energies; the black arrow indicates the energy corresponding with formation of Kr $^1S_0$ + ground state Ar^+ ion.

The angular distributions of the Ar photofragments formed after predissociation of the two-photon-excited ArKr states of both electronic bands are to some extent anisotropic; Ar photofragments in the inner ring of the images recoil primarily along the laser polarization vector. The angular distribution of the fragments in the outer ring, which corresponds to fragments formed after three-photon absorption, can be modeled fairly accurately using a single anisotropy parameter, $\beta_2 = 2$, neglecting the higher order terms. Using eq 6, somewhat better fits to the angular distributions shown in Figure 6C and 7C are obtained with $\beta_2 = 2, \beta_4 = 0.03, \beta_6 = 0$, and $\beta_2 = 2, \beta_4 = 0.05, \beta_6 = 0.05$, respectively. This modeling indicates that the dissociation at the three-photon level is fast, and the Ar photofragments recoil with a nearly $\cos^2 \theta$ angular distribution around the laser polarization vector. The Ar photofragment ion images reveal that $\mu-v$ correlation leads already to anisotropic fragment distributions for predissociation at the two-photon level. However, part of the $\mu-v$ correlation cancels out in the three-photon absorption/dissociation process (process 11) because no higher order terms are needed to describe the angular distributions of the Ar photofragments in the outer ring.

Conclusions

We have studied the photodissociation and photoionization dynamics of Kr_2 and ArKr, using the photofragment ion imaging technique. Several electronic states excited by two-photon resonant absorption are investigated. Our photofragment ion imaging study reveals various competitive channels in the dissociation and ionization dynamics of these two-photon-excited states. In general, all two-photon resonant excited states studied predissociate. This predissociation, however, competes with processes in which a third photon is absorbed. Three-photon absorption leads to ionization of the molecule or to dissociation of highly excited states, into two neutral fragments. The relative contributions of these processes depend on the particular electronic state studied and the laser fluences used. Transitions in ArKr, which were previously assigned to states in which the Kr moiety is electronically excited,[10,19] are shown to be transitions in which the Ar moiety is electronically excited.

Acknowledgment. A.J.R.H. thanks the Associated Western Universities, Inc., for an AWU-DOE fellowship. This work was supported by the U.S. Department of Energy, Office of Basic Energy Sciences, Division of Chemical Sciences, and in part by the U.S. National Science Foundation under NSF CHE-9322690. We would like to thank E. Audouard and F. Spiegelmann for supplying numerical values of the potential energy surfaces of Kr_2 and ArKr.

References and Notes

(1) McCusker, M. In *Excimer Lasers*; Rhodes, C. K., Ed.; Springer: Berlin, 1984; p 47.

(2) Kurosawa, K.; Takigawa, Y.; Sasaki, W.; Okuda, M.; Fujiwara, E.; Yoshida, K.; Kato, Y. *IEEE J. Quantum Electron.* **1991**, *27*, 71.

(3) Efthimiopoulos, T.; Stoicheff, B. P. *IEEE J. Quantum Electron.* **1992**, *28*, 1439.

(4) Sato, F.; Sunada, Y.; Okamoto, S.; Kannari, F. *Appl. Phys. Lett.* **1992**, 1378.

(5) Mulliken, R. S. *J. Chem. Phys.* **1970**, *52*, 5170.

(6) Castex, M. C.; Morlais, M.; Spiegelmann, F.; Malrieu, J. P. *J. Chem. Phys.* **1981**, *75*, 5006.

(7) Spiegelmann, F.; Gadea, F. X.; Castex, M. C. *Chem. Phys.* **1990**, *145*, 173.

(8) Audouard, E.; Spiegelmann, F. *J. Chem. Phys.* **1991**, *94*, 6102.

(9) Mizukami, Y.; Nakatsuji, H. *J. Chem. Phys.* **1990**, *92*, 6084.

(10) Tanaka, Y.; Yoshino, K.; Freeman, D. E. *J. Chem. Phys.* **1973**, *59*, 5160.

(11) Cheshnovsky, O.; Gedanken, A.; Raz, B.; Jortner, J. *Chem. Phys. Lett.* **1973**, *22*, 23.

(12) LaRoque, P. E.; Lispon, R. H.; Herman, P. R.; Stoicheff, B. P. *J. Chem. Phys.* **1986**, *84*, 6627.

(13) Lipson, R. H.; LaRoque, P. E.; Stoicheff, B. P. *J. Chem. Phys.* **1985**, *82*, 4470.

(14) Herman, P. R.; LaRocque, P. E.; Stoicheff, B. P. *J. Chem. Phys.* **1988**, *89*, 4535.

(15) Madej, A. A.; Stoicheff, B. P. *Phys. Rev. A* **1988**, *38*, 3456.

(16) Pratt, S. T.; Dehmer, P. M.; Dehmer, J. L. *J. Chem. Phys.* **1985**, *83*, 5380.

(17) Pratt, S. T.; Dehmer, P. M.; Dehmer, J. L. *Chem. Phys. Lett.* **1985**, *116*, 245.

(18) Dehmer, P. M.; Pratt, S. T.; Dehmer, J. L. *J. Chem. Phys.* **1986**, *85*, 13.

(19) Dehmer, P. M.; Pratt, S. T. *J. Chem. Phys.* **1988**, *88*, 4139.

(20) Echt, O.; Cook, M. C.; Castleman, A. W., Jr. *J. Chem. Phys.* **1987**, *87*, 3276.

(21) Dimov, S. S.; Cai, J. Y.; Lipson, R. H. *J. Chem. Phys.* **1994**, *101*, 10313.

(22) Koeckhoven, S. M.; Buma, W. J.; De Lange, C. A. *J. Chem. Phys.* **1995**, *102*, 4020.

(23) Lipson, R. H.; Dimov, S. S.; Cai, J. Y.; Wang, P.; Bascal, H. A. *J. Chem. Phys.* **1995**, *102*, 5881.

(24) Richmann, M. K.; Nelson, T. O.; Setser, D. W. *Chem. Phys. Lett.* **1993**, *210*, 71.

(25) Ediger, M. N.; Eden, J. G. *Chem. Phys. Lett.* **1986**, *126*, 158.

(26) Ediger, M. N.; Eden, J. G. *J. Chem. Phys.* **1986**, *85*, 1757.

(27) Kane, D. J.; Eden, J. G. *Chem. Phys. Lett.* **1988**, *144*, 71.

(28) Kane, D. J.; Abele, C. C.; Fraser, R. D.; Shannon, D. C.; Eden, J. G.; Ginter, M. L. *J. Chem. Phys.* **1993**, *99*, 99.

(29) Ng, C. Y.; Trevor, D. J.; Mahan, B. H.; Lee, Y. T. *J. Chem. Phys.* **1976**, *66*, 446.

(30) Huber, K. P.; Herzberg, G. *Constants of Diatomic Molecules*; Van Nostrand Reinhold Co.: New York, 1979.

(31) Ng, C. Y.; Tiedemann, P. W.; Mahan, B. H.; Lee, Y. T. *J. Chem. Phys.* **1977**, *66*, 5737.

(32) Dehmer, P. M.; Pratt, S. T. *J. Chem. Phys.* **1982**, *77*, 4804.

(33) Dehmer, P. M.; Poliakoff, E. D. *Chem. Phys. Lett.* **1981**, *77*, 326.

(34) Kitsopoulos, T. N.; Buntine, M. A.; Baldwin, D. P.; Zare, R. N.; Chandler, D. W. *Science* **1993**, *260*, 1605.

(35) Heck, A. J. R.; Chandler, D. W. *Ann. Rev. Phys. Chem.* **1995**, *46*, 335.

(36) Chandler, D. W.; Houston, P. L. *J. Chem. Phys.* **1987**, *87*, 1445.

(37) Thoman, J. W., Jr.; Chandler, D. W.; Parker, D. H.; Janssen, M. H. M. *Laser Chem.* **1988**, *9*, 27.

(38) Pratt, S. T.; Dehmer, P. M. *Chem. Phys. Lett.* **1982**, *87*, 533.

(39) Dehmer, P. M.; Pratt, S. T.; Dehmer, J. L. *J. Chem. Phys.* **1987**, *91*, 2593.

(40) Aymar, M.; Coulombe, M. *At. Data Nucl. Tables* **1978**, *21*, 537.

(41) Chang, R. S. F.; Horiguchi, H.; Setser, D. W. *J. Chem. Phys.* **1980**, *73*, 778.

(42) Cannon, B. D.; Glab, W. L.; Ogarzalek-Loo, R. *Phys. Rev. A* **1993**, *47*, 147.

(43) Sugar, J.; Musgrove, A. *J. Phys. Chem. Ref. Data* **1991**, *20*, 859.

(44) Zare, R. N. *Mol. Photochem.* **1972**, *4*, 1.

(45) Sander, R. K.; Wilson, K. R. *J. Chem. Phys.* **1975**, *63*, 4242.

(46) Kawasaki, M.; Sato, H.; Kikuchi, T.; Fukuroda, A.; Kobayashi, S.; Arikawa, T. *J. Chem. Phys.* **1987**, *86*, 4425.

(47) Sato, T.; Kinugawa, T.; Arikawa, T.; Kawasaki, M. *Chem. Phys.* **1992**, *165*, 173.

(48) Yang, C. N. *Phys. Rev.* **1948**, *74*, 764.

(49) Buntine, M. A.; Baldwin, D. P.; Chandler, D. W. *J. Chem. Phys.* **1992**, *96*, 5843.

(50) Bobetic, M. V.; Barker, J. A. *J. Chem. Phys.* **1976**, *64*, 2367.

(51) Piper, L. G.; Setser, D. W.; Clyne, M. A. A. *J. Chem. Phys.* **1975**, *63*, 5018.

(52) Moore, C. E. *Atomic Energy Levels*; Nat. Bur. Stds.: Washington, DC, 1947; Vol. Circ. 467.

JP9520207